Supplementary Material

Formation of a stable LiF-rich SEI layer on molybdenum-based MXene electrodes for enhanced lithium metal batteries

Shakir Zaman[1], Mugilan Narayanasamy[1], Shabbir Madad Naqvi[1], Tufail Hassan[1], Aamir Iqbal[1], Ujala Zafar[1], Noushad Hussain[1], Seunghwan Jeong[1], Soo Yeong Cho[1], Sungmin Jung[1], Chong Min Koo[1,2,*]

[1]School of Advanced Materials Science and Engineering, Sungkyunkwan University, Gyeonggi-do 16419, Republic of Korea.
[2]School of Chemical Engineering, Sungkyunkwan University, Gyeonggi-do 16419, Republic of Korea.

Correspondence to: Dr. Chong Min Koo, School of Advanced Materials Science and Engineering, Sungkyunkwan University, Seobu-ro 2066, Jangan-gu, Suwon-si, Gyeonggi-do 16419, Republic of Korea. E-mail:chongminkoo@skku.edu

XPS Analysis

The deconvoluted C 1s, F 1s, O 1s, and Ti 2p XPS profiles of the Mo_2CT_x and $Mo_2TiC_2T_x$ MXenes are provided in [**Supplementary Figure 4** and **5**]. In the C 1s region, the observed peaks at (281.86, 284.56, 285.97, and 287.92) eV correspond to Mo–C, C−C, C−H, and C−O species, respectively. The F 1s region is fitted with a single component at a BE of 685.03 eV, corresponding to an −F surface termination. For the O 1s region in Mo_2CT_x, the peaks at (529.72, 531.22, and 532.37) eV are assigned to Mo_2CO_x, $Mo_2C{-}OH_x$, and $Mo_2C(OH_x)$ $-H_2O_x$, respectively [**Supplementary Figure 4**]. In the C 1s region of $Mo_2TiC_2T_x$, the peak at 282.88 eV is attributed to C atoms bonded to both Mo and Ti atoms (Mo–C/Ti–T_x), while the peaks at (284.61, 285.91, and 287.48) eV are associated with C−C, C−H, and C−O species, respectively. The F 1s region is fitted by a single component at a BE of 684.95 eV, corresponding to F–

terminations. In the O 1s region, the peak at 530.01 is attributed to Molybdenum oxides (Mo/Ti–O), while peaks at (531.41 and 532.59) eV are assigned to C–Mo–OH_x species. The Ti 2p region displays peaks at (455.82, 456.78, 458.39, and 464.23) eV that correspond to Ti–C, Ti^{2+}, Ti^{3+}, and TiO_2 (Ti^{4+}), respectively [**Supplementary Figure 5**]. For $Mo_2Ti_2C_3T_x$, the Ti 2p peaks at (455.72, 456.96, and 458.63) correspond to the C−Ti^{+}, Ti^{2+}, and Ti^{3+} bonds, respectively. Furthermore, the C 1s peaks at (282.96, 284.61, 286.18, and 287.98) eV are ascribed to the Ti–C–Mo, C−C, CH_x, and C−O bonds, respectively. Additionally, the XPS spectra for the O 1s and F 1s indicate that the $Mo_2Ti_2C_3T_x$ contains Mo/Ti atoms covalently bonded to surface terminal groups, such as −O, −OH, and −F [**Supplementary Figure 6**].

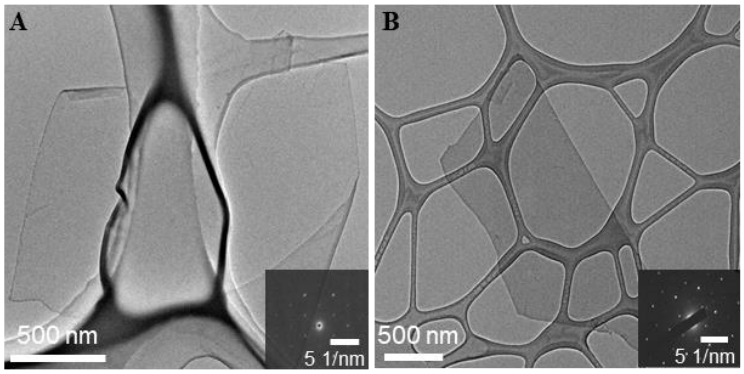

Supplementary Figure 1. HR−TEM images of the (A) $Mo_2TiC_2T_x$ and (B) Mo_2CT_x MXene sheets.

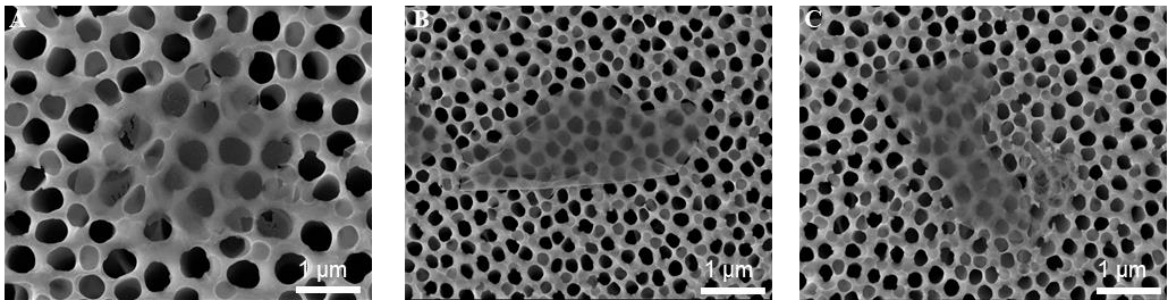

Supplementary Figure 2. Single flake SEM imagery of the (A) $Mo_2Ti_2C_3T_x$, (B) $Mo_2TiC_2T_x$, and (C) Mo_2CT_x MXene sheets.

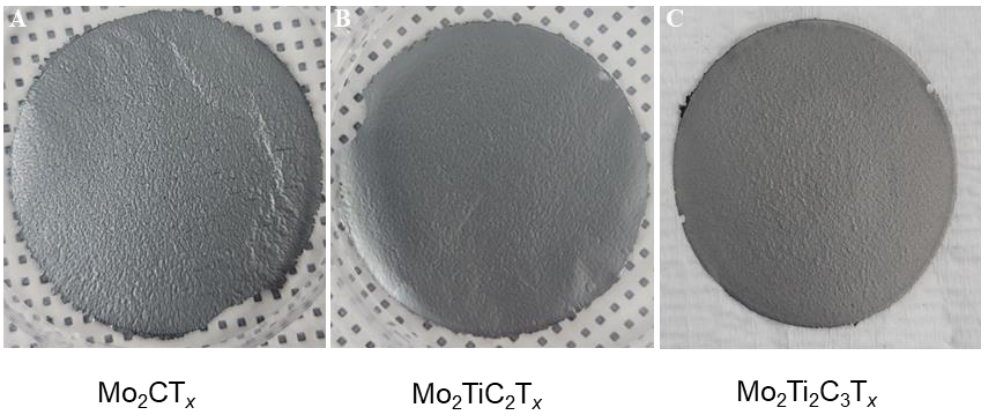

Supplementary Figure 3. Photographs of the vacuum-filtered (A) Mo_2CT_x, (B) $Mo_2TiC_2T_x$, and (C) $Mo_2Ti_2C_3T_x$ MXene films.

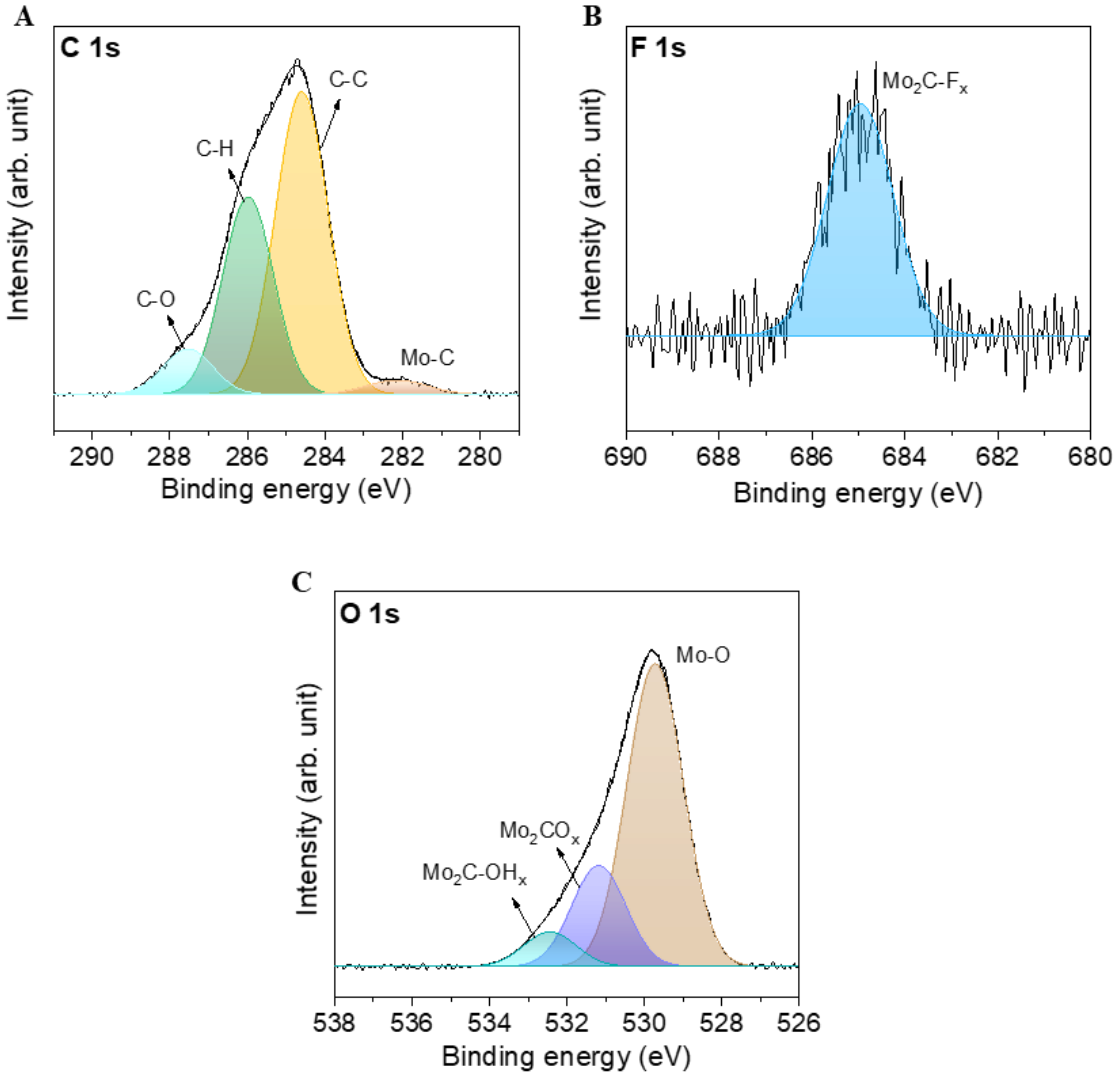

Supplementary Figure 4. (A) C 1s, (B) F 1s, and (C) O 1s XPS spectra of the Mo_2CT_x MXene.

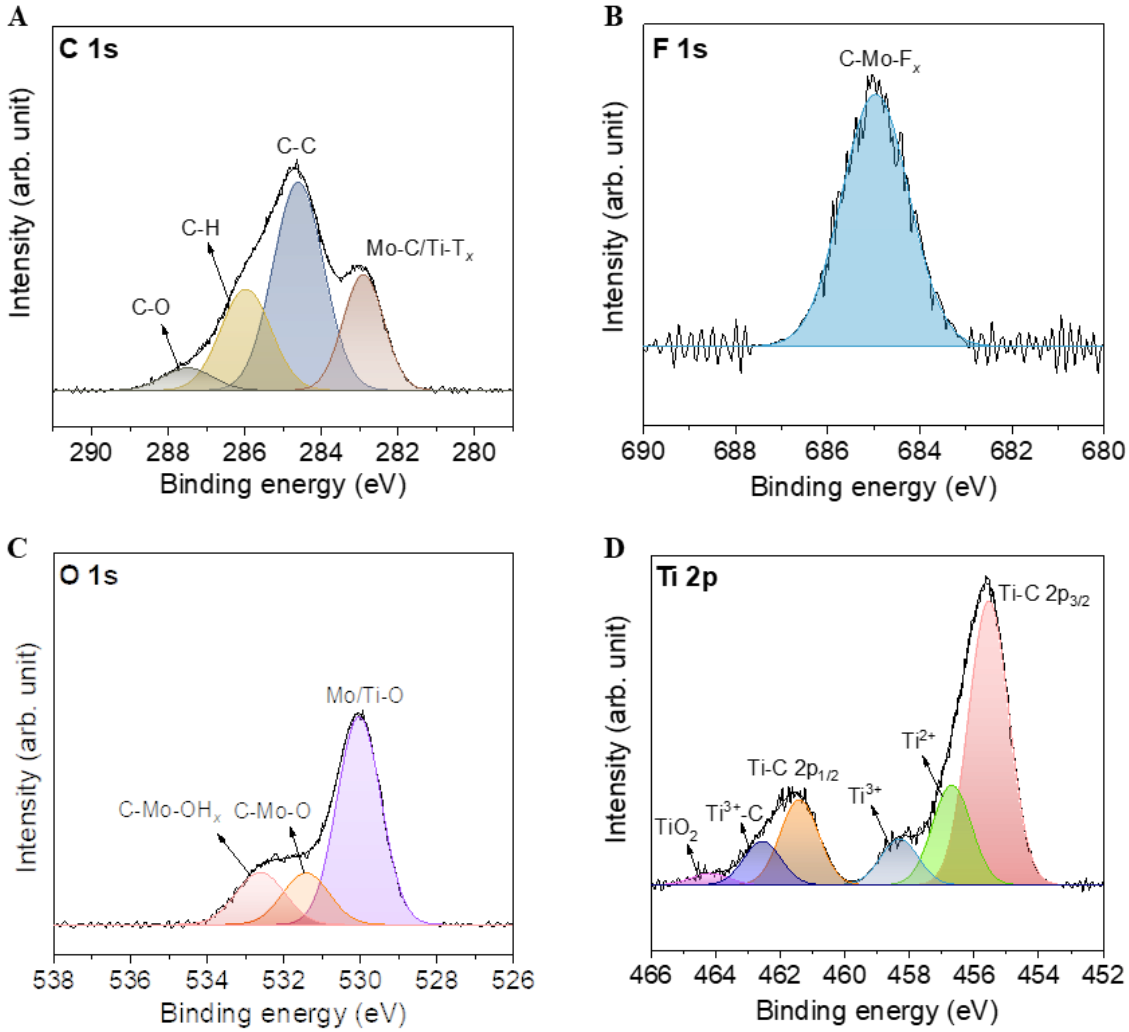

Supplementary Figure 5. (A) C 1s, (B) F 1s, (C) O 1s, and (D) Ti XPS spectra of the $Mo_2TiC_2T_x$ MXene.

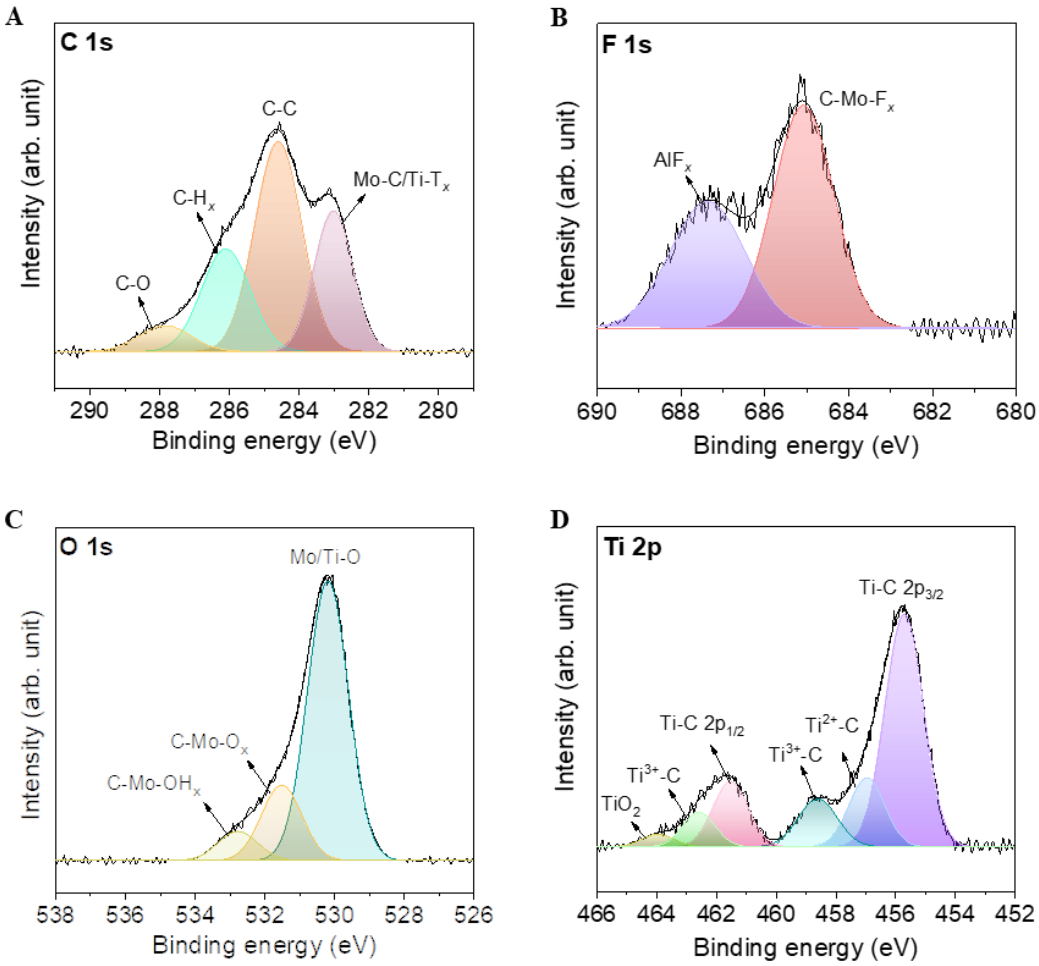

Supplementary Figure 6. (A) C 1s, (B) F 1s, (C) O 1s, and (D) Ti XPS spectra of the $Mo_2Ti_2C_3T_x$ MXene.

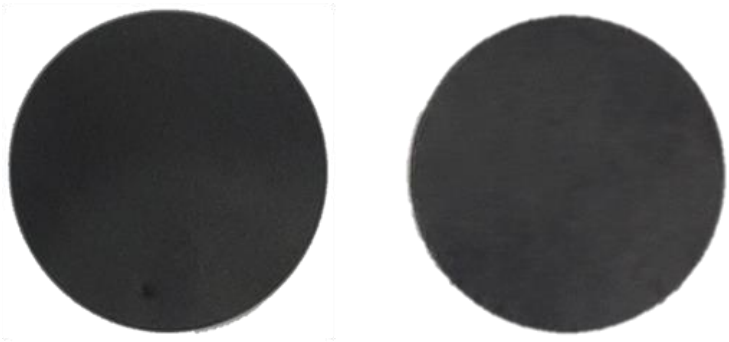

Supplementary Figure 7. Optical imagery of the $Mo_2TiC_2T_x$, and Mo_2CT_x powder coated Cu electrodes.

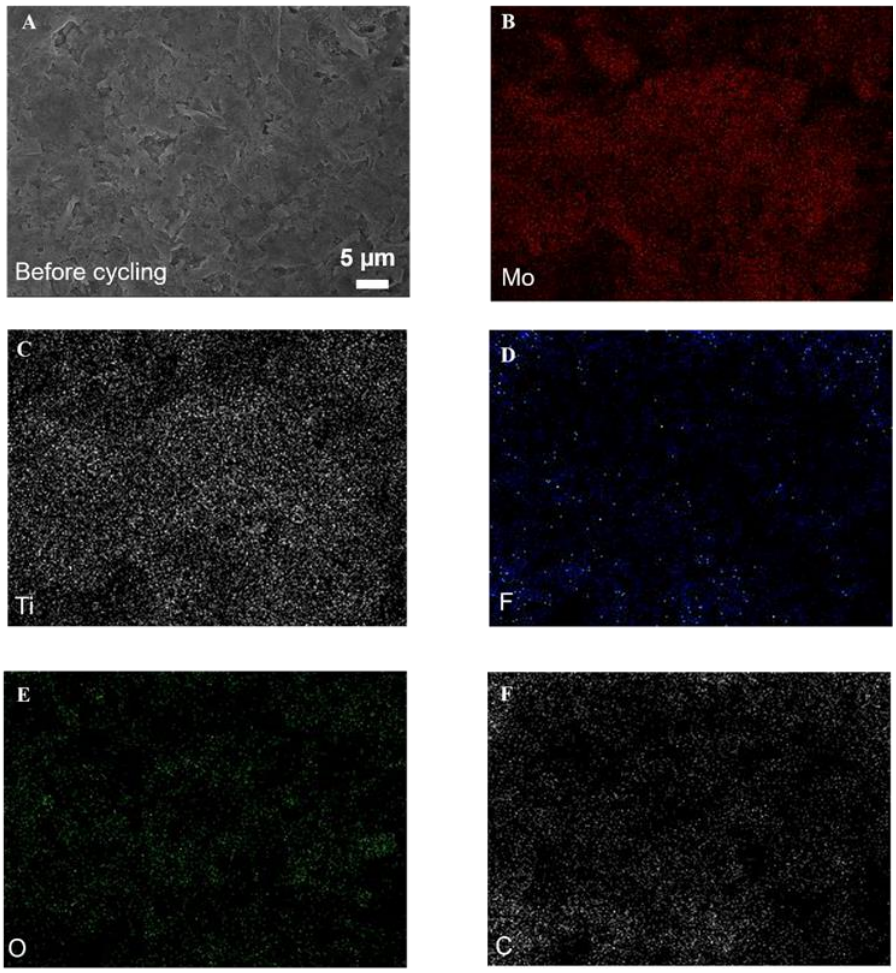

Supplementary Figure 8. (A) Top-view SEM image of the surface of $Mo_2Ti_2C_3T_x$-Cu. (B) Mo, (C) Ti, (D) F, (E) O, and (F) C EDS mapping on the surface of $Mo_2Ti_2C_3T_x$-Cu.

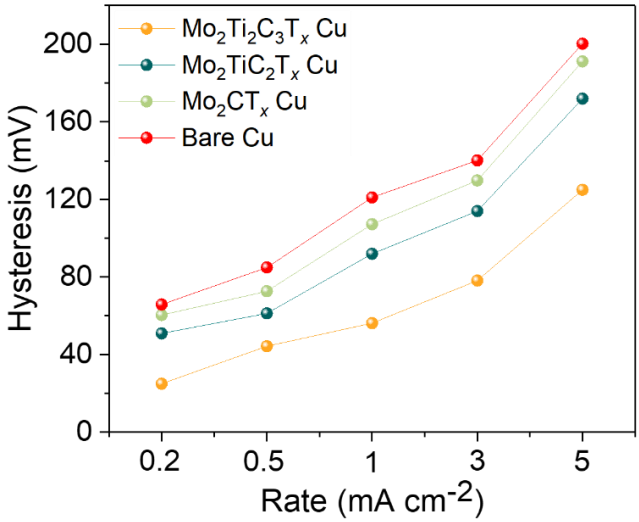

Supplementary Figure 9. Rate performance comparison at different current densities of (0.2, 0.5, 1, 3, and 5) $mA \cdot cm^{-2}$.

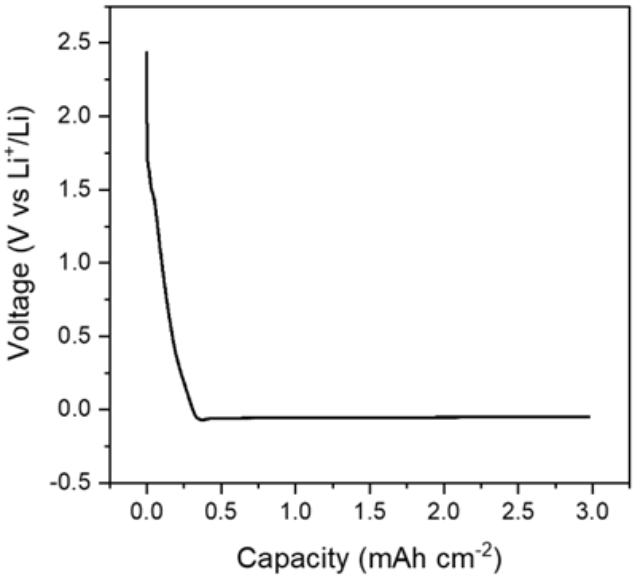

Supplementary Figure 10. The voltage profile for 3 mAh cm^{-2} Li deposition on anode in half-cell configuration.

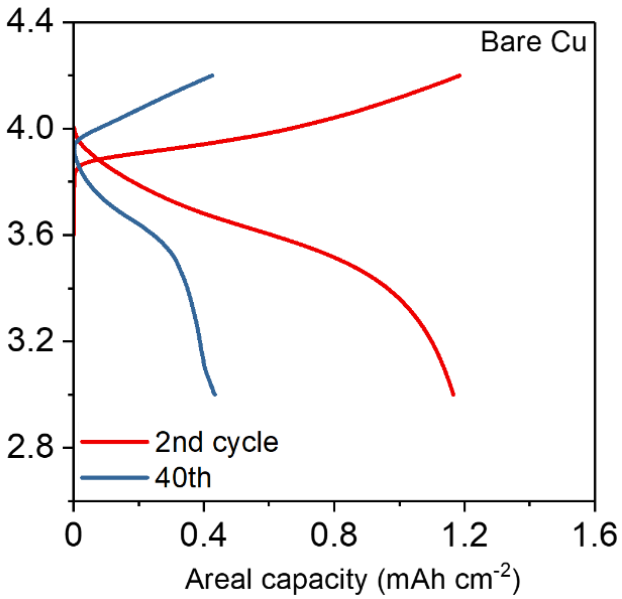

Supplementary Figure 11. The voltage profile for the Li-bare Cu//NCM622.

Supplementary Table 1. XPS elemental concentration of $Mo_2Ti_2C_3T_x$, $Mo_2TiC_2T_x$, and Mo_2CT_x films.

Element ratio (Atomic %)	Mo	Ti	C	O	F
$Mo_2Ti_2C_3T_x$	16.943	9.354	43.781	21.422	5.214
$Mo_2TiC_2T_x$	20.975	7.367	40.731	20.391	3.041
Mo_2CT_x	24.341	-	50.098	22.421	1.397

Supplementary Table 2. Comparison summary of the half-cell performance of the $Mo_2Ti_2C_3T_x$ Cu with the previously reported literature.

Materials	Test conditions	LMB performance	Electrolyte	Ref.
LASS−Cu//Li	1 mAh cm^{-2}, 3 mA cm^{-2}	70 cycles, CE: 96.27 %	1M LiTFSI in (DOL)/(DME) (V/V = 1:1) with 2 wt.% $LiNO_3$	[1]
Cu–Ag	1 mAh cm^{-2}, 3 mA cm^{-2}	200 cycles, CE: 98.23 %	1M LiTFSI in (DOL)/(DME) (V/V = 1:1) with 1 wt.% $LiNO_3$	[2]
Nitrogen–carbon Cu nanorod	1 mAh cm^{-2}, 5 mA cm^{-2}	30 cycles, CE: 90 %	1M LiTFSI in (DOL)/(DME) (V/V = 1:1) with 0.1M $LiNO_3$	[3]
3D porous Copper	1 mAh cm^{-2}, 5 mA cm^{-2}	50 cycles, CE: 98.7 %	1M LiTFSI in (DOL)/(DME) (V/V = 1:1) with 1 wt.% $LiNO_3$	[4]
ZnO−Cu mesh	1 mAh cm^{-2}, 5 mA cm^{-2}	70 cycles, CE: 95 %	0.6M LiTFSI in (DOL)/(DME) (V/V = 1:1) with 0.4 wt.% $LiNO_3$	[5]
PNIPAM polymer Cu	1 mAh cm^{-2}, 5 mA cm^{-2}	150 cycles, CE: 90 %	1M LiTFSI in (DOL)/(DME) (V/V = 1:1) with 2 wt.% $LiNO_3$	[6]
$Ti_3C_2T_x$ Cu	1 mAh cm^{-2}, 5 mA cm^{-2}	160 cycles, CE: 90 %	1M LiTFSI in (DOL)/(DME) (V/V = 1:1) with 2 wt.% $LiNO_3$	[7]
$Mo_2Ti_2C_3T_x$ Cu	**1 mAh cm^{-2}, 3 mA cm^{-2}**	**544 cycles, CE: 99.79 %**	**1M LiTFSI in (DOL)/(DME) (V/V = 1:1) with 5 wt.% $LiNO_3$**	**This work**
$Mo_2Ti_2C_3T_x$ Cu	**1 mAh cm^{-2}, 5 mA cm^{-2}**	**298 cycles, CE: 98.15 %**	**1M LiTFSI in (DOL)/(DME) (V/V = 1:1) with 5 wt.% $LiNO_3$**	**This work**

Supplementary Table 3. Comparison of electrochemical performance of $Mo_2Ti_2C_3T_x$ with $Mo_2Ti_2C_3T_x$, Mo_2CT_x, and a bare Cu reference sample.

Material	Nucleation overpotential (mV)	Cycling stability and CE (1 mAh cm^{-2})		EIS (Ω)	Full cell performance		Ref
		3 mA cm^{-2}	5 mA cm^{-2}	After 200 cycles	Initial discharge capacity (mAh cm^{-2})	Capacity retention (After 100 cycles)	
$Mo_2Ti_2C_3T_x$	13	544 (99.79 %)	298 (98.15 %)	11.5	1.64	70 %	
$Mo_2Ti_2C_3T_x$	16	402 (98.14 %)	248 (97.5 %)	13	1.24	48 %	**This work**
Mo_2CT_x	21	282 (96.91 %)	206 (96.78 %)	26	1.19	37 %	
Bare Cu	32	143 (96.24 %)	99 (95.32 %)	44	1.16	35 %	

Supplementary Table 4. Comparison summary of full cell performance of the $Mo_2Ti_2C_3T_x$ Cu||NCM622 with the literature.

Cell Condition	Electrolyte	Initial Capacity	Capacity Retention	Ref.
Cu@Sn||$LiNiCoAlO_2$	1M $LiPF_6$ in FEC/EMC (1/4, WT/WT)	1.0 mAh cm^{-2}	~C/2 charge/discharge, ~0 % after 80 cycles	[8]
3DLN||LFP	1M $LiPF_6$ in EC/DMC (1/1, v/v)	1.5 mAh cm^{-2}	C/3 charge/discharge, 65.1 % after 50 cycles	[9]
Cu||LFP	1M LiTFSI + 2M LiFSI in (DOL)/(DME) (V/V = 1:1) with 3 wt.% $LiNO_3$	0.85 mAh cm^{-2}	39 % after 100 cycles	[10]
Cu||LFP	1M LiTFSI + 2M LiFSI in (DOL)/(DME) (1:1, v/v)	1.5 mAh cm^{-2}	~C/8 charge/discharge, ~50 % after 50 cycles	[11]
Cu||LNMO	7M LiFSI in FEC	1.43 mAh cm^{-2}	~54 % after 50 cycles	[12]
$Mo_2Ti_2C_3T_x$ Cu||NCM622	**1M $LiPF_6$ in EC/DMC (1/1, v/v)**	**1.64 mAh cm^{-2}**	**~C/2 charge/discharge, ~70 % after 100 cycles**	**This work**

References

1. Kwon HM, Kim NH, Hong SJ, Sim WH, Lee M, Son S, Bae KY, Kim JY, Youn DH, Kim YS. Uniform Li-metal growth on renewable lignin with lithiophilic functional groups derived from wood for high-performance Li-metal batteries. *Surfaces and Interfaces* 2024;44:103643. https://doi.org/10.1016/j.surfin.2023.103643

2. Cui S, Zhai P, Yang W, Wei Y, Xiao J, Deng L, Gong Y. Large-scale modification of commercial copper foil with lithiophilic metal layer for Li metal battery. *Small* 2020;16:1905620. 10.1002/smll.201905620

3. Yin D, Huang G, Wang S, Yuan D, Wang X, Li Q, Sun Q, Xue H, Wang L, Ming J. Free-standing 3D nitrogen–carbon anchored Cu nanorod arrays: in situ derivation from a metal–organic framework and strategy to stabilize lithium metal anodes. *Journal of Materials Chemistry A* 2020;8:1425-31. https://doi.org/10.1039/C9TA10772J

4. Lin H, Zhang Z, Wang Y, Zhang XL, Tie Z, Jin Z. Template-sacrificed hot fusion construction and nanoseed modification of 3D porous copper nanoscaffold host for stable-cycling lithium metal anodes. *Advanced Functional Materials* 2021;31:2102735. https://doi.org/10.1002/adfm.202102735

5. Huang S, Zhang W, Ming H, Cao G, Fan L-Z, Zhang H. Chemical energy release driven lithiophilic layer on 1 m2 commercial brass mesh toward highly stable lithium metal batteries. *Nano Letters* 2019;19:1832-7. https://doi.org/10.1021/acs.nanolett.8b04919

6. Li N, Ye Q, Zhang K, Yan H, Shen C, Wei B, Xie K. Normalized lithium growth from the nucleation stage for dendrite-free lithium metal anodes. *Angewandte Chemie* 2019;131:18414-9. https://doi.org/10.1002/ange.201911267

7. Yang D, Zhao C, Lian R, Yang L, Wang Y, Gao Y, Xiao X, Gogotsi Y, Wang X, Chen G. Mechanisms of the planar growth of lithium metal enabled by the 2D lattice confinement from a Ti3C2Tx MXene intermediate layer. *Advanced Functional Materials* 2021;31:2010987. https://doi.org/10.1002/adfm.202010987

8. Zhang SS, Fan X, Wang C. A tin-plated copper substrate for efficient cycling of lithium metal in an anode-free rechargeable lithium battery. *Electrochimica Acta* 2017;258:1201-7. https://doi.org/10.1016/j.electacta.2017.11.175

9. Liu M, Li X, Shao C, Han C, Liu Y, Li X, Ma X, Chen F, Liu Y. Synchronous-ultrahigh conductive-reactive N-atoms doping strategy of carbon nanofibers networks for high-performance flexible energy storage. *Energy Storage Materials* 2022;44:250-62. https://doi.org/10.1016/j.ensm.2021.10.025

10. Qiu F, Li X, Deng H, Wang D, Mu X, He P, Zhou H. A concentrated ternary-salts electrolyte for high reversible Li metal battery with slight excess Li. *Advanced Energy Materials* 2019;9:1803372. https://doi.org/10.1002/aenm.201803372

11. Beyene TT, Bezabh HK, Weret MA, Hagos TM, Huang C-J, Wang C-H, Su W-N, Dai H, Hwang B-J. Concentrated dual-salt electrolyte to stabilize Li metal and increase cycle life of anode free Li-metal batteries. *Journal of The Electrochemical Society* 2019;166:A1501-A9. 10.1149/2.0731908jes

12. Suo L, Xue W, Gobet M, Greenbaum SG, Wang C, Chen Y, Yang W, Li Y, Li J. Fluorine-donating electrolytes enable highly reversible 5-V-class Li metal batteries. *Proceedings of the National Academy of Sciences* 2018;115:1156-61. https://doi.org/10.1073/pnas.1712895115